ChemistrySelect

Research Article
doi.org/10.1002/slct.202405073

Chemistry Europe
European Chemical Societies Publishing

www.chemistryselect.org

Zero-Waste Production of Copper Nanoparticles and Activated Carbon from *Erigeron canadensis* L.: A Sustainable Approach for Environmental and Health Applications

Erdi Can Aytar,[a] Taşkın Basılı,[b] Alper Durmaz,[c] Betül Aydın,[d] Rukan Can Seyfeli,[e] İbrahim Mizan Kahyaoğlu,[b] and Selcan Karakuş*[f, g]

This study presents a novel, zero-waste process for producing copper nanoparticles (CuNPs), activated carbons (ACs), and oil extract (OE) from a plant *Erigeron canadensis* L. in Sp. Pl.: 863 (1753). This method optimizes resource utilization and eliminates waste, offering a sustainable approach to green synthesis. The NPs were characterized using XRD, SEM, and FTIR. Their effectiveness was evaluated through comparative studies on methylene blue removal, antioxidant capacity, and antibacterial activity. The prepared OE exhibited superior antibacterial properties, particularly against *Klebsiella pneumoniae subsp*. pneumoniae ATCC 13883 (inhibition zone: 19 ± 0 mm) and *Proteus vulgaris* RSKK 96029 (inhibition zone: 18.7 ± 0.6 mm). The AC demonstrated exceptional dye adsorption efficiency, ranging from 98.62% to 99.50%. Antioxidant tests revealed that CuNPs possessed strong antioxidant capacity, with an IC_{50} of 0.023 ± 0.002 mg/mL in the DPPH radical scavenging test and 0.41 ± 0.07 mg/mL in the iron chelation test. The OE demonstrated lower DPPH scavenging capacity (0.43 ± 0.01) but significant iron-chelating ability (41.94 ± 1.06). In comparison, standard antioxidants EDTA and BHT showed lower effectiveness in their respective tests. These experimental findings underscore the potential of this green approach for bio zero-waste-derived products in environmental and biomedical applications, highlighting its broad applicability.

1. Introduction

With increasing consumption and rapid urban growth, persistent pollutants such as harmful microorganisms and inorganic and organic chemicals pose significant threats to water quality and public health in aquatic ecosystems. The accumulation of wastewater and restricted access to safe drinking water have significantly reduced the availability of clean water. In the context of zero waste in safe drinking water, the aim is to create a sustainable environmental solution that minimizes environmental issues while ensuring access to clean water without causing secondary pollution.[1,2] In contrast to the conventional standard methods, which include chemical, physical, and biological processes, zero waste-based nanotechnology is thought to be a green and environmentally friendly way to remove different types of hazardous compounds from wastewater.[3]

Modern multifunctional materials, particularly those derived from plants, are increasingly in demand due to their superior properties such as biocompatibility, renewability, eco-friendliness, versatility, and high performance.[4] In addition, these green materials, such as adsorbents, antioxidants, or antimicrobials, take part in the removal of pollution from the aqueous environment.[5–10] However, with the zero-waste approach utilizing multifunctional plant residues, extracts, and essential oils, there is a growing demand for advanced features such as residue-free purification, drug delivery systems, water purification, and sensor technologies.[11–13] *Erigeron canadensis* L. also known as *Conyza canadensis* or *Leptilon canadense*, is a plant native to North America and recognized as an invasive species. It typically grows in disturbed areas like roadsides, wastelands, and slopes. Traditionally, *E. canadensis* has been used in herbal medicine to treat various conditions such as indigestion, obesity, hepatitis, enteritis, swollen lymph nodes, blood in the urine, malaria, and acute inflammation. The plant contains bioactive compounds including pyromeconic acid (PY), terpenoids, sterols, flavonoids, and organic acids. However, further studies are needed to fully understand its potential anticancer effects and safety.[14]

[a] *E. C. Aytar*
Faculty of Agriculture, Department of Horticulture, Uşak University, Usak 64200, Türkiye

[b] *T. Basılı, İ. M. Kahyaoğlu*
Faculty of Science, Department of Chemistry, Ondokuz Mayıs University, Samsun 55139, Türkiye

[c] *A. Durmaz*
Ali Nihat Gökyiğit Botanical Garden Application and Research Center, Artvin Çoruh University, Artvin 08000, Türkiye

[d] *B. Aydın*
Faculty of Science, Department of Biology, Gazi University, Ankara 06500, Türkiye

[e] *R. C. Seyfeli*
Faculty of Engineering, Department of Chemical Engineering, Ondokuz Mayıs University, Samsun 55139, Türkiye

[f] *S. Karakuş*
Faculty of Engineering, Department of Chemistry, Istanbul University-Cerrahpaşa, Istanbul 34320, Türkiye
E-mail: selcan@iuc.edu.tr

[g] *S. Karakuş*
Health Biotechnology Joint Research and Application Center of Excellence, Esenler, Istanbul 34220, Türkiye

The flowering parts of *E. canadensis* have been widely used in traditional medicine for their diuretic, tonic, antifungal, and astringent properties. Beyond traditional uses, the plant is also recognized in modern medicine for its ability to stop bleeding, promote urine production, relieve diarrhea, and act as an astringent and deworming agent. The plant's aqueous extracts are rich in antioxidants and antiplatelet compounds, which contribute to its medicinal value. Additionally, the ethanolic extract is sold in Poland under the brand name Hemorigen, available in tablet and tincture forms. This product is commonly used to control excessive bleeding, especially in gynecological and hemorrhoidal conditions, with tannins believed to be the key active ingredients.[14,15]

Many phytochemicals present in plant extracts, such as ascorbic acids, phenols, aldehydes, amides, flavones, carboxylic acids, and terpenoids, have the ability to reduce metal ions into metal NPs. Numerous distinctions exist between the surface, chemical, biological, optical, thermal, and electrical properties of green metal and metal oxide NPs compared to their respective bulk metals.[16–18] Adaptable green inorganic metal NPs, including silver, gold, copper, iron, platinum, and palladium, have recently been the focus of extensive research. Copper plays an important role in human health and ensures the balance and stability of tissues. It has a strong antibacterial, antifungal, antioxidant, and anticancer effect. Copper nanoparticles (CuNPs) rapidly accumulate in colloidal environments and easily mix with macromolecules to form copper oxide, which retains some of its physical and chemical properties over time. Green CuNPs have demonstrated potent antibacterial activity against a wide range of micro-organisms, such as *Staphylococcus aureus*, *Pseudomonas aeruginosa*, and *Escherichia coli*. Experimental results show that bacterial viability percentages decrease depending on the amount in the presence of NPs.[19] The potency of CuNPs against bacteria and fungi is increased by their high surface-to-volume ratio. Metal ions released into solutions and direct contact with microbes are the sources of their antibacterial activity. Additionally, the noticeable band gap that CuNPs have enhances their visual qualities and promotes their antibacterial activity. According to absorption studies, this characteristic is influenced by their distinct shape, nanoscale size, and high surface area.[20] The utilization of plant extracts in the synthesis of CuNPs has been demonstrated to enhance their antimicrobial activity. This green synthesis approach has been demonstrated to offer an eco-friendly and cost-effective method, while also leveraging the natural reducing and stabilizing agents present in plant extracts. These agents have been shown to improve the antimicrobial efficacy of the nanoparticles. The enhanced activity is attributed to the unique properties imparted by the plant extracts, such as the presence of bioactive compounds that can synergize with the nanoparticles.[21,22]

Activated carbons (ACs) are particularly useful for a variety of adsorption procedures due to their huge surface area and porous structure, which confer high dye adsorption capabilities. Owing to their inherent qualities, ACs are in great demand and are utilized extensively throughout the world. Their numerous uses include wastewater treatment, environmental remediation, and other industrial operations. They are also employed in the biobased product trend. The literature has reported on the adsorption of pollutants such as dyes,[23] drugs,[24] heavy metals,[25] phenolic compounds,[26] and pesticides[27] using ACs from different sources. There are currently no studies that simultaneously exhibit antioxidant properties, destroy microorganisms (*Klebsiella pneumoniae* subsp. *pneumoniae* ATCC 13883 and *Proteus vulgaris* RSKK), and rapidly remove methylene blue dye using Erigeron-derived chemicals with a zero-waste approach. This study introduces a novel zero-waste process for producing CuNPs, ACs, and OE from *E. canadensis* plants. The green strategy optimized resource use and eliminated waste, offering a sustainable synthesis approach. Characterizations were performed using X-ray diffraction (XRD), scanning electron microscopy (SEM), AI-enhanced SEM, and Fourier-transform infrared spectroscopy (FTIR). The biobased products were evaluated for methylene blue removal, antioxidant capacity, and antibacterial activity. The OE exhibited strong antibacterial properties against *Klebsiella pneumoniae* (inhibition zone: 19 ± 0 mm) and Proteus vulgaris (inhibition zone: 18.7 ± 0.6 mm). The AC showed excellent methylene blue adsorption efficiency (98.62%–99.50%), while CuNPs demonstrated high antioxidant capacity with an IC50 of 0.023 ± 0.002 mg/mL in the DPPH test and 0.41 ± 0.07 mg/mL in the iron chelation test. The AC had lower DPPH scavenging capacity (0.43 ± 0.01) but significant iron-binding ability (41.94 ± 1.06). Compared to EDTA and BHT, these results highlight the potential of this green synthesis approach for bio zero-waste-derived products in environmental and biomedical applications.

2. Materials and Methods

2.1. Materials

E. canadensis specimens were collected from densely populated and undisturbed areas within the Ondokuz Mayıs University Campus. The above-ground parts (including stems, leaves, and flowers) of the plants were harvested during their flowering period, which spans from June to November, and subsequently identified by Dr. Alper Durmaz. These specimens have been cataloged in the Herbarium of the Biology Department at Ondokuz Mayıs University under accession number OMUB-6860.

The freshly collected plant material was subjected to a drying process in a laboratory oven at 45 °C for 72 h. Following desiccation, the plant material was finely ground using a blender and stored in airtight bags. These samples are kept in a controlled environment, protected from moisture and heat, until they are ready for further analysis and synthesis.

2.2. Preparation of E. canadensis Extract-Based CuNPs

2.2.1. Preparation of E. canadensis Extract

A 40 g portion of the resulting dry homogenate was soaked in 400 mL of ethanol for 48 h. The plant residue was separated from the solution by decantation and left to dry for subsequent use in

activated carbon synthesis. The ethanol was then removed from the extraction solution using a rotary evaporator.[28] Finally, 1 g of the dried solid extract was dissolved in 50 mL of ethanol to prepare the *E. canadensis* extract solution.

2.2.2. Preparation of CuNPs

A 30 mL solution of $CuSO_4$ containing 1 mol of Cu^{2+} was mixed with a 1 M thioacetamide (CH_3CSNH_2) solution, added dropwise until the total volume reached 50 mL. The resulting mixture was subjected to ultrasonic treatment for 15 min. Next, 50 mL of the Erigeron extract solution was added dropwise to the colloidal mixture, which was then sonicated for an additional 15 min. Following this, the mixture was further sonicated for an additional 15 min, and then centrifuged at 3000 rpm for 30 min. The precipitate was collected and dried at 100 °C for 5 h to complete the synthesis of the CuNPs.

2.3. Preparation of E. canadensis Extract-Based Activated Carbon and E. canadensis Extract-Based Oil

The above-ground parts of *E. canadensis* were harvested during their flowering period for use in the extraction process. The residue remaining from the extraction process was utilized for the synthesis of activated carbon. Hydrochar was generated by introducing 10 g of these dried samples into a batch reactor operating at a temperature of 700 °C for a duration of 4 h. Following the reaction, the reactor was rapidly cooled by submerging it in cold water, and the resulting slurry, representing the hydrochar, was collected. After this initial cooling and collection step, the hydrochar is considered to be prepared as the base material for activated carbon. Subsequently, the hydrochars underwent another 24-h drying period at 110 °C to ensure their readiness for further applications. It is noteworthy that steam was generated during the reaction, which was subsequently condensed to yield a liquid oil-based product. This liquid product will be subjected to analysis to assess its antioxidant and antimicrobial potential.

2.4. Adsorption Studies

Adsorption studies were conducted by testing the adsorption of methylene blue dye on activated carbon synthesized from *E. canadensis* waste. Initially, an aqueous solution of methylene blue (Sigma-Aldrich) with a concentration of 1000 mg L^{-1} was prepared and used as a primary standard. Adsorption solutions were then prepared by diluting this standard solution to concentrations of 1000, 750, 500, 250, and 100 mg L^{-1}. The adsorption process was carried out using 20 mL of each of these solutions. In all adsorption experiments, a constant 0.1 g of activated carbon was used as the adsorbent. Measurements were taken at 5-min intervals during experiments conducted at 20, 30, and 40 °C, with all experiments concluding at the 30-min mark.

2.5. Determination of Antioxidant Capacity

2.5.1. DPPH (2,2-Diphenyl-1-Picrylhydrazyl) Assay

Modifications were made based on the procedure of Ref. [29]. The free radical scavenging potentials of the CuNPs and OE samples were determined using the DPPH assay. For this test, various concentrations of 1 mL sample were mixed with an ethanol solution of DPPH radical (0.1 mM) in a tube. The mixture was left to incubate in the dark at room temperature for 30 min. Subsequently, the absorbance was measured at 517 nm using a UV spectrophotometer against a blank. The butylated hydroxytoluene (BHT) was used as the standard. All measurements were performed in triplicate. The following Equation (1) was employed to ascertain the percentage of DPPH radical scavenging inhibition.

$$\text{DPPH scavenging activity (\% inhibition)} = \left[\frac{(Absorbance_{control}) - (Absorbance_{sample})}{Absorbance_{control}}\right] \times 100 \quad \text{(Eq 1)}$$

The construction of a sample concentration curve was undertaken with the objective of determining the sample concentration that would be required to result in a 50% reduction in the initial DPPH concentration. In the context of linear regression analysis, the resulting calculated value is designated as IC_{50}.

2.5.2. Determination of Ferrous Ion Chelating Capacity

The ferrous ion chelating capacity of the CuNPs and OE samples was determined according to the method mentioned in Ref. [30] Varying concentrations of the extract were mixed with 135µL of the solvent. 2 mM $FeCl_2$ was added to the solution and incubated for 5 min. After that, five mM ferrozine solution was added and lasted 10 min. After incubation, absorbance was measured at 562 nm by using a spectrophotometer (Thermo Scientific Varioskan Flash) against a blank. As a reference standard, ethylenediaminetetraacetic acid (EDTA) was used. All measurements were performed in triplicate. The percentage of ferrous ion inhibition was determined by employing the following Equation (2):

$$\text{Ferrous ion chelating (\% inhibition)} = \left[\frac{(Absorbance_{control}) - (Absorbance_{sample})}{Absorbance_{control}}\right] \times 100 \quad \text{(Eq 2)}$$

A sample concentration curve was constructed to determine the sample concentration required to result in a 50% reduction in the initial ferrous ion concentration. In the context of linear regression analysis, the resulting calculated value is designated as IC_{50}.

2.6. Antimicrobial Effects of E. canadensis Cu-NPs and OE

2.6.1. Test Microorganisms

Ten bacterial strains were used for antimicrobial activity. The bacterial strains were *E. coli* ATCC 35218, *S. aureus* subsp. *aureus* ATCC 25923, *Salmonella enterica* subsp. *enterica* serovar Typhimurium ATCC 14028, *Pseudomonas aeruginosa* ATCC 27853, *Bacillus cereus* ATCC 14579, *Klebsiella pneumoniae* subsp. *pneumoniae* ATCC 13883, *S. aureus* subsp. *aureus* ATCC 43300 (Methicillin-resistant *S. aureus*-MRSA), *Enterococcus faecalis* ATCC 51299 (Drug-resistant *Enterococcus faecalis*-DRE), *Proteus vulgaris* RSKK 96029, and *Enterococcus faecalis* ATCC 29212.

2.6.2. Antimicrobial Activity

The antimicrobial activity of the samples was evaluated by following the Clinical and Laboratory Standards Institute (CLSI) guidelines for the disc diffusion method (CLSI, 2015). Before the experimental procedure, the bacterial strains were cultivated on Tryptic Soy Agar at 37 °C for 24 h. Following the incubation period, bacterial suspensions (1–1.5 × 10^8 CFU/mL) were prepared in sterile saline (0.85% NaCl) (w/v) solution in accordance with the 0.5 McFarland standard. Bacterial suspensions were inoculated onto Mueller–Hinton agar plates. Sterile paper discs (6 mm in diameter) were impregnated with 10 µL of each sample and negative control, then dried at room temperature. The discs were positioned on the agar plates that had been inoculated, and the plates were incubated at 37 °C for 24 h. Following the incubation period, the diameters of the inhibition zones were measured. All tests were conducted in triplicate, and the inhibition zones were calculated as means ± standard deviations.

2.7. Calculations Part

Several XRD mathematical models, including the Debye–Scherrer equation (Equations 1,2), the modified Scherrer model (Equation 3), the Williamson–Hall model (Equation 4), and the Halder–Wagner model (Equation 5), were applied, and the compatibility of the data with these models, as well as the crystal sizes identified by each model, are presented.[31–34]

$$D = \frac{K\lambda}{\beta \cos\theta} \tag{1}$$

$$\varepsilon = \frac{\beta \cos\theta}{4} \tag{2}$$

$$\ln \beta = \ln \frac{K\lambda}{D} + \ln \frac{1}{\cos\theta} \tag{3}$$

$$\beta_{hkl} \cos\theta = \varepsilon 4 \sin\theta + \frac{K\lambda}{D} \tag{4}$$

$$\left(\frac{\beta^*_{hkl}}{d^*_{hkl}}\right)^2 = \frac{1}{D}\frac{\beta^*_{hkl}}{d^{*2}_{hkl}} + \left(\frac{\varepsilon}{2}\right)^2 \tag{5}$$

where *D*: size, *K*: constant, λ: wavelength of the X-ray radiation, β: line width at half maximum height, θ: Bragg's angle, $\mathcal{E}$: Microstrain, *d*: D-spacing, and *hkl* are the miller indices.

2.8. Characterization

The Thermo UV–vis spectrophotometer (USA) was employed to record absorption spectra, while FT-IR studies were conducted using the FT-IR spectrometer (Perkin Elmer Spectrum Two Model, Germany) with a spectral range of 400–4000 cm^{-1}, known for its exceptional accuracy in measuring infrared radiation. The XRD spectra were obtained using a Rigaku Smart Lab X-Ray Diffractometer at a scan rate of 0.2 degrees per minute, within a 2θ range of 30° to 80°. The shape factor (K) and XRD wavelength (λ) values, obtained from the analysis center, were used in the calculation with values of 0.89 and 0.154, respectively. İn the BET study N_2 physisorption analysis was conducted to examine the porous structure of *E. canadensis* under the 5 mmHg N_2 pressure.

3. Results and Discussion

3.1. Characterization of the Erigeron-Based CuNPs (EC-CuNPs), ACs, and OE

The Figure 1 presented various surface characterization results of CuNPs synthesized from *E. canadensis*. Figure 1(a) showed a SEM image of the EC-CuNPs, providing a general view of their morphology at 30000x magnification. Figure 1(b) featured an AI-enhanced SEM image displayed in 16-bit/Rainbow RGB mode, which accentuated the morphological features of the EC-CuNPs. In Figure 1(c), an advanced AI-based topographical analysis was illustrated, where a 3D surface plot was overlaid on the SEM image, utilizing a grid size of 512, smoothing factor of 6.0, perspective angle of 0.52, and lighting intensity of 0.43 to deliver a more detailed surface characterization. Finally, Figure 1(d) included a color histogram derived from the SEM results, representing the distribution of nanoparticle sizes.

The O-H stretching vibration is detected at 3200 cm^{-1}, while the CH_3 symmetric stretching appears at 2980 cm^{-1}. The CH_2 symmetric stretching, along with its asymmetric counterpart, is observed in the range of 2920–2850 cm^{-1}. The peak corresponding to the amide I band is located at 1630 cm^{-1}, whereas the amide II band is identified within the 1560–1530 cm^{-1} region. The esterified CH_3 group contributes to signals between 1350 and 1450 cm^{-1}, and the C-O stretching vibration manifests in the 1300–1000 cm^{-1} range.[35–38]

The FTIR spectra presented in Figure 2 illustrate the functional chemistry of the *Erigeron*-based CuNPs and ACs. In Figure 2a, the broad bands detected in the 3500–3000 cm^{-1} range are typically attributed to the stretching vibrations of O-H and N-H bonds, corresponding to hydroxyl and amine groups within the sample. Additionally, a symmetric CH_3 stretching band is observed at 2980 cm^{-1}, alongside symmetric and asymmetric CH_2 stretching bands at 2920–2850 cm^{-1}. Medium-intensity peaks corresponding to C-O stretching vibrations are found in

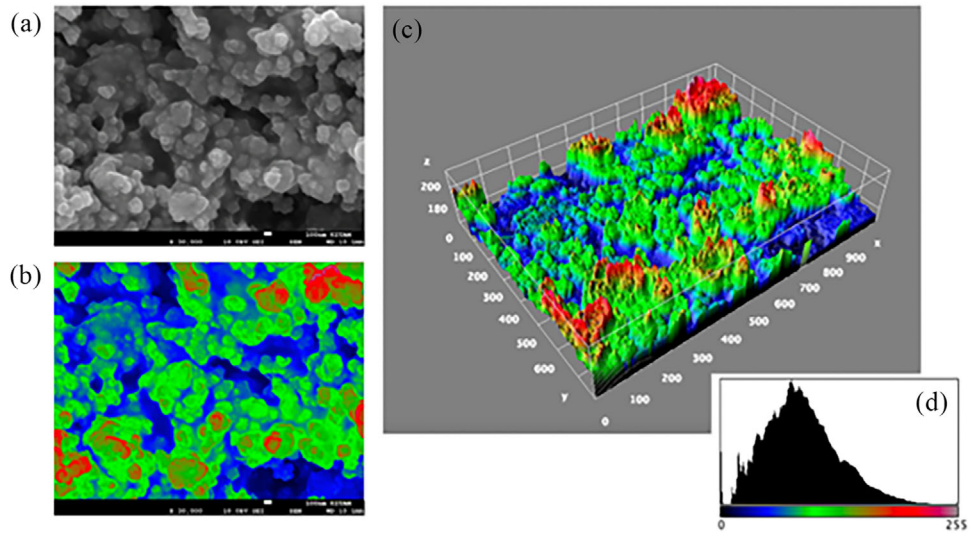

Figure 1. a) SEM image of *E. canadensis* based CuNPs (EC-CuNPs), b) AI-enhanced SEM image (16-bit/Rainbow RGB mode), c) AI-enhanced SEM image with 3D surface plot (grid size 512, smoothing 6.0, perspective 0.52, lighting 0.43), and d) TEM color histogram.

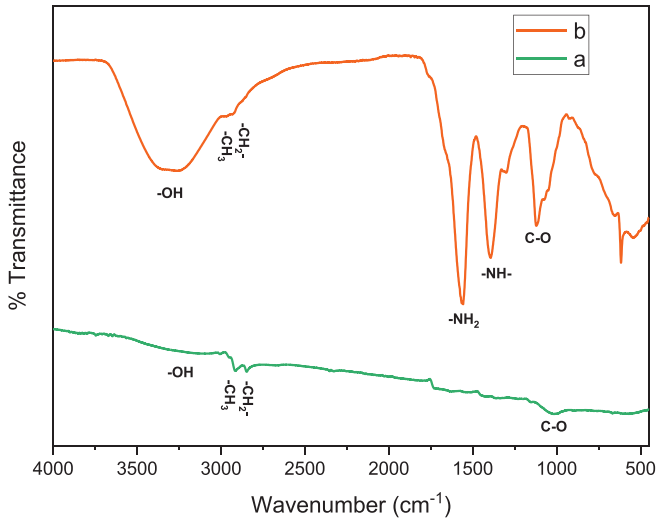

Figure 2. FTIR spectra of a) *E. canadensis* based CuNPs, and b) ACs.

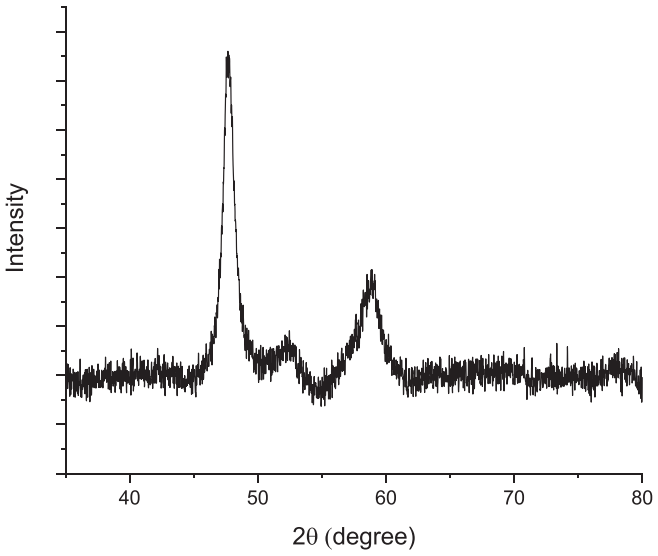

Figure 3. XRD graph of the *E. canadensis* based CuNPs.

the 1300–1000 cm^{-1} region. Additionally, the FTIR spectrum of EC-CuNPs reveals peaks at 667, and 572 cm^{-1}, all of which are indicative of the production of Cu, as depicted in Figure 2a. In Figure 2b, for the ACs, an O-H stretching band is observed at 3200 cm^{-1}, a symmetric CH_3 stretching band at 2980 cm^{-1}, and symmetric and asymmetric CH_2 stretching bands at 2920–2850 cm^{-1}. The amide I peak is observed at 1630 cm^{-1}, while the amide II band appears between 1560 and 1530 cm^{-1}. Peaks for the esterified CH_3 group are present in the 1350–1450 cm^{-1} range, and C-O stretching vibrations are observed between 1300 and 1000 cm^{-1}.[35–38]

The XRD graph of the *Erigeron*-based CuNPs showed three main peaks of 32°, 59°, and 77° (Figure 3), whereas the major peak positions at 2θ values of 49° in the high angle XRD of the *Erigeron*-based CuNPs indicate the existence of cubic centered crystalline nature of NPs (Figure 3). The value of the crystallite size obtained by Debye–Scherrer, Modified Scherrer model, Williamson–Hall model, and Halder–Wagner model were obtained using Figure 3, and compared in Table 1. The crystallite sizes of the *Erigeron*-based CuNPs were determined to be 10.03, 29.85, 4.02, and 64.10 nm using the DebyeScherrer equation, Modified Scherrer model, Williamson–Hall model, and Halder–Wagner model, respectively (Figure 4). The size calculated by

Table 1. Particle size and R^2 results of XRD models for the *E. canadensis* based CuNPs.

Model	R^2	Size (nm)
Debye–Sherrer Equation	–	10.03
Modified Shrrer model	0.9979	29.85
Williamson–Hall model	0.9496	4.02
Halder–Wagner model	0.9913	64.10

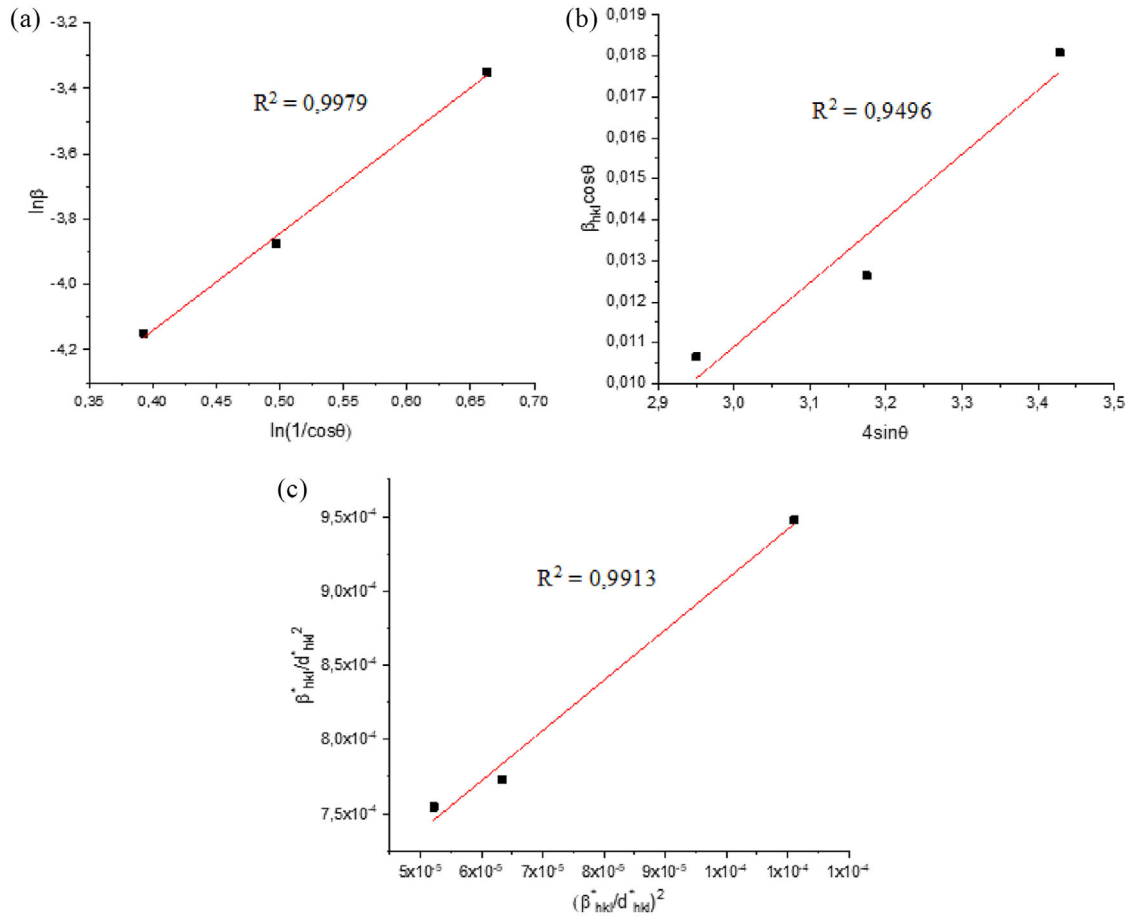

Figure 4. XRD model graphs for the *E. canadensis* based CuNPs a) Modified Sherrer model, b) Williamson– Hall model, and c) Halder–Wagner model.

the Debye–Scherrer method (10.03 nm) is more than double the value obtained by the Williamson–Hall model (4.02 nm) but is approximately three times smaller than the value derived from the Modified Scherrer model (29.85 nm) and about six times smaller than the size calculated by the Halder–Wagner model (64.10 nm). A reduction in crystallite size for metal and metal oxide NPs, as determined by the Scherrer method, has also been reported in the literature.[39]

Table 2. Antioxidant activity of different samples: DPPH radical scavenging and iron chelating capacities.

Sample Name	DPPH (IC_{50} mg/mL)	Iron Chelating (IC_{50} mg/mL)
E. canadensis CuNPs	0.023 ± 0.002	0.41 ± 0.07
OE	0.43 ± 0.01	41.94 ± 1.06
EDTA	–	5.30 ± 4.44
BHT	96.47 ± 0.54	–

3.2. Antioxidant and Antimicrobial Activity

Antioxidant activity tests were conducted to evaluate the free radical scavenging and iron chelation capacities of various samples, as presented in Table 2. The *E. canadensis* CuNPs and OE sample demonstrated high efficacy in the DPPH radical scavenging test, with an IC_{50} value of 0.023 ± 0.002 mg/mL. It was observed that *E. canadensis* CuNPs sample had better free radical scavenging effect than BHT (IC_{50} value 96.47 ± 0.54 mg/mL) used as positive control. This low IC_{50} value indicates that the *E. canadensis* nanoparticles effectively scavenge DPPH radicals, revealing a strong antioxidant capacity. In the iron chelation test, it also exhibited a notable performance with an IC_{50} value of 0.41 ± 0.07 mg/mL, suggesting its ability to effectively bind iron ions and thus reduce iron-induced oxidative damage. This effect was observed to be higher than EDTA (IC_{50} value 5.30 ± 4.44 mg/mL) as positive control. On the other hand, the Oil Derived from Activated Carbon (OE) sample showed an efficacy of 0.43 ± 0.01 (percentage of substance) in the DPPH radical scavenging test, indicating that the biowaste sample has a relatively low DPPH radical scavenging capacity, and therefore, lower effectiveness. In the iron chelation test, the biowaste sample exhibited a significant iron-binding capacity with an IC_{50} value of 41.94 ± 1.06. However, while a low IC_{50} value denotes higher effectiveness, a high percentage of substance provides indirect information about effectiveness in this context. EDTA was tested in the iron chelation assay with an IC_{50} value of 5.30 ± 4.44 mg/mL, which suggests that EDTA has lower effectiveness in iron chelation compared to the CuNPs BHT (Butylated

Hydroxytoluene), on the other hand, showed a considerably high IC_{50} value of 96.47 ± 0.54 mg/mL in the DPPH radical scavenging test. This result indicates that BHT has low free radical scavenging capacity and is less effective compared to the other tested samples.

In the study evaluating the antioxidant activity of *E. canadensis* CuNPs, the IC_{50} value for the DPPH free radical scavenging test was determined to be 0.023 ± 0.002 mg/mL. This high antioxidant activity indicates that the nanoparticles possess strong free radical scavenging properties. Comparing these results with other studies reveals significant findings.

In the literature, there are quite a number of studies indicating that copper nanoparticles (CuNPs) show significant antioxidant activity attributed to their ability to scavenge reactive oxygen species (ROS) and reduce oxidative stress. This property makes them promising candidates for various biomedical applications, including the management of oxidative stress-related conditions. The antioxidant properties of these CuNPs are primarily evaluated through their ability to scavenge free radicals, which is a crucial function in preventing oxidative stress-related damage in biological systems. In the study by Venugopalan et al., the DPPH radical scavenging activity of *Borreria hispida* (Linn.) extract copper nanoparticles (CuNPs) were reported with an IC_{50} value of 0.6 µg/mL (approximately 0.0006 mg/mL).[40] This indicates higher antioxidant activity compared to *E. canadensis* NPs, highlighting the effective neutralization of free radicals by CuNPs. In the study by Hasheminya and Dehghannya, the DPPH free radical scavenging activity of *Eryngium caucasicum* Trautv aqueous extracts CuNPs was found to be 40.02%, while *E. canadensis* NPs demonstrated this activity at 58.98%.[41] This result shows that *E. canadensis* NPs have superior antioxidant efficacy compared to CuNPs, which could be attributed to the higher concentrations of phenolic compounds and flavonoids.

Golinejad et al. evaluated the antioxidant activities of gold nanoparticles in *Taxus baccata* (AuNPs), but specific IC_{50} values were not provided. This study investigated the effects of gold nanoparticles (AuNPs) on antioxidant enzyme activity. The activity of the catalase (CAT) enzyme significantly increased in cells treated with AuNPs compared to control cells. The highest CAT activity was observed at a concentration of 2 µg/mL AuNPs and 24 h of exposure. However, this increase was not observed at the same concentration after 8 h. The findings suggest that AuNPs may support defense mechanisms against oxidative stress in plants. The CAT enzyme protects plants from oxidative damage by breaking down hydrogen peroxide (H_2O_2) into oxygen and water. The expression of specific isoenzymes (isozymes) of CAT is crucial for plant survival under environmental stresses. The study concludes that an increase in CAT activity during stress is necessary to maintain the plant's defense system. Compared to our study, although IC_{50} values were not provided, it is evident that gold nanoparticles are more effective.[42] In the study by Shanmugapriya et al., the antioxidant activity of CuNPs in *Withania somnifera* was found to be 62%, suggesting that *E. canadensis* NPs possess higher antioxidant capacity. Additionally, the IC_{50} value for CuNPs in Shanmugapriya et al.'s study was 51.53 µg/mL, which supports the superior antioxidant efficacy of *E. canadensis* NPs.[43] In the study by Rajeskumar et al., CuNPs' *Cissus arnotiana* antioxidant properties were compared to ascorbic acid, with CuNPs showing maximum antioxidant properties equivalent to ascorbic acid at 40 µg/mL.[44] These values indicate that the antioxidant activity of *E. canadensis* NPs is higher compared to CuNPs. In a study conducted by Maulana et al. in 2022, they examined the antioxidant activity of copper nanoparticles synthesized using methanol extracts obtained from *Anonnaceae squamosa* leaves and found that the IC_{50} value was 263.35 ppm. Although the antioxidant activity of plant extract-derived CuNPs is promising, it is essential to consider the variability in activity based on the type of plant extract and synthesis conditions. The selection of plant extract has been demonstrated to exert a significant influence on the dimensions, morphology, and surface chemistry of the nanoparticles, thereby modulating their biological activity. Further research is required to optimize synthesis methods and to achieve a comprehensive understanding of the mechanisms underlying their antioxidant properties.

Table 3. Antibacterial activity of *E. canadensis* CuNPs and OE against various bacterial strains (Inhibition Zones in mm).

Bacteria Strain	*E. canadensis* CuNPs	OE
	100 mg/mL	Direct
E. coli ATCC 35218	ND	9 ± 0
S. aureus subsp. *aureus* ATCC 25923	ND	9 ± 0
Salmonella enterica subsp. *enterica* serovar Typhimurium ATCC 14028	8 ± 0	9 ± 0
Pseudomonas aeruginosa ATCC 27853	8 ± 0	11 ± 0
Bacillus cereus ATCC 14579	ND	11.5 ± 0.7
Klebsiella pneumoniae subsp. *pneumoniae* ATCC 13883	ND	19 ± 0
MRSA	9 ± 0	13.5 ± 0.7
VRE	9 ± 0	11.7 ± 0.6
Proteus vulgaris RSKK 96029	8 ± 0	18.7 ± 0.6

ND: Not detected

Antibacterial activity tests evaluated the effects of *E. canadensis* CuNPs and bio waste samples on various bacterial strains, as shown in Table 3 and Figure 5. No inhibition zones were observed for *E. canadensis* NPs against bacterial strains such as *E. coli* ATCC 35218, *S. aureus* subsp. *aureus* ATCC 25923, and *B. cereus* ATCC 14579. However, bio waste demonstrated a 9 mm inhibition zone against these strains.

For *S. enterica* subsp. *enterica serovar Typhimurium* ATCC 14,028 and *P. seudomonas aeruginosa* ATCC 27,853, *E. canadensis* nanoparticles showed inhibition zones of 8 mm, while bio waste provided inhibition zones of 9 mm. In the case of *K. pneumoniae* subsp. *pneumoniae* ATCC 13,883, bio waste achieved a 19 mm inhibition zone, whereas *E. canadensis* nanoparticles did not show any inhibition zone. For MRSA and VRE strains, inhibition zone of 9 mm was observed in CuNPs. Biowaste oil affected the MRSA and VRE strains with inhibition zones of 13.5 ± 0.7 mm and 11.7 ± 0.6, respectively.

Research Article
doi.org/10.1002/slct.202405073
Chemistry Europe
European Chemical Societies Publishing

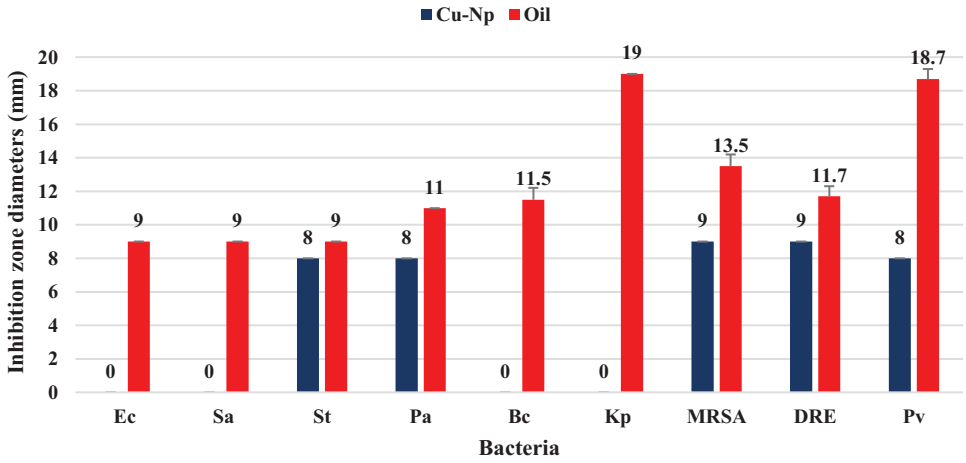

Figure 5. Antimicrobial activities of the samples (Ec: *E. coli* ATCC 35218; Sa: *S. aureus* subsp. aureus ATCC 25923; St: *Salmonella enterica* subsp. enterica serovar Typhimurium ATCC 14028; Pa: *Pseudomonas aeruginosa* ATCC 27853; Bc: *Bacillus cereus* ATCC 14579; Kp: *Klebsiella pneumoniae* subsp. pneumoniae ATCC 13883; MRSA: Methicillin-resistant *S. aureus* subsp. aureus ATCC 43300; DRE: Drug-resistant *Enterococcus faecalis* ATCC 51299; and Pv: *Proteus vulgaris* RSKK 96029; usage concentrations of the samples: CuNPs: 100 mg/mL; Oil: Direct).

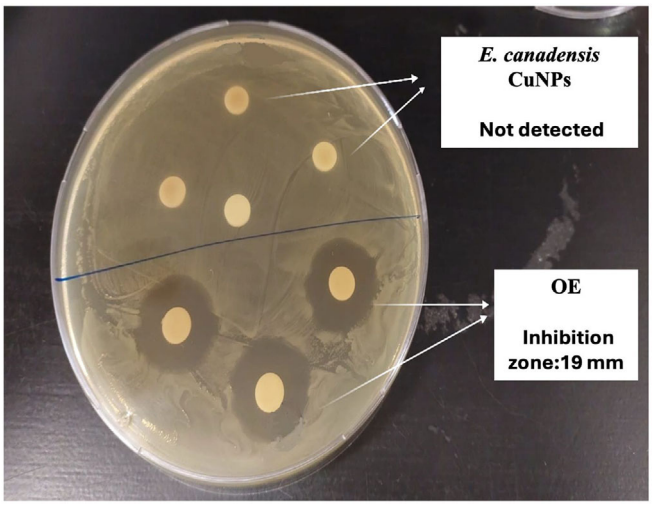

Figure 6. Inhibition Zones of OE and *E. canadensis* CuNPs Against *Klebsiella pneumoniae* subsp. *pneumoniae*.

In *P. vulgaris* RSKK 96029, bio waste resulted in an 18.7 ± 0.6 mm inhibition zone, while *E. canadensis* CuNPs showed an 8 ± 0 mm inhibition zone. These antibacterial activity results indicate that the bio waste sample is effective against a broad bacterial spectrum, whereas the *E. canadensis* CuNPs exhibit activity against some strains but do not show as broad an effect as bio waste.

The antimicrobial effect of the samples on different pathogenic bacteria was examined by disc diffusion method and the inhibition zone diameters obtained are shown in Figure 6. As a result of statistical analyses with the data obtained, it was determined that the antimicrobial activity of the OE was higher than the CuNPs ($p < 0.0001$). The OE demonstrated antimicrobial activity against all bacterial strains examined, whereas CuNPs exhibited efficacy against only five. The efficacy of CuNPs against MRSA and DRE, which are antibiotic-resistant bacteria, indicates that this nanoparticle has antimicrobial potential.

It is established that CuNPs produced via the use of plant extracts demonstrate antimicrobial properties. CuNPs have attracted considerable interest, particularly in recent years, due to their potent antimicrobial properties. Several different mechanisms can be put forward to explain the antimicrobial effects of CuNPs. Copper nanoparticles have been observed to bind to the cell membrane of microorganisms, leading to disruption of the membrane's structural integrity. These mechanisms include the disruption of the cell membrane structure,[45] the triggering of reactive oxygen species production,[46] the infliction of damage to proteins and DNA,[47] and the creation of a toxic effect accompanied by the release of copper ions.[48]

OE, which is derived from a variety of organic materials through pyrolysis, contains a complex mixture of substances. The key components identified across the studies are hydrocarbons, phenols, alcohols, amines, and organosulfur compounds,[49,50] It has been demonstrated that pyrolysis oil derived from diverse biomass sources, including *Muli bamboo* and *Pinus densiflora*, displays considerable inhibitory efficacy against a spectrum of pathogenic bacteria, such as *Salmonella* and *E. coli*,[51,52] The mechanism of action entails the disruption of the bacterial cell membrane integrity, which results in the leakage of cellular materials and a subsequent loss of viability. Furthermore, the presence of phenolic compounds and other secondary metabolites in pyrolysis oil contributes to its antimicrobial properties, thereby enhancing its effectiveness against both Gram-positive and Gram-negative bacteria.[53] The diverse range of bioactive compounds and their respective modes of action indicate that pyrolysis oil has considerable potential as a natural preservative for foodstuffs, and as a natural antimicrobial agent. A literature review revealed no previous studies investigating the antimicrobial effect of pyrolysis oil obtained from the *E. canadensis* plant extract pulp. This study has demonstrated the potential of pyrolysis oil derived from this plant species to function as an antimicrobial agent.

The results evaluating the antibacterial activity of *E. canadensis* OE demonstrate effectiveness against a broad spectrum of

Table 4. % Uptake list in different conditions of MB adsorption for *E. canadensis* AC.

20 °C		30 °C		40 °C	
Initial Concentration (mg L^{-1})	% Uptake	Initial Concentration (mg L^{-1})	% Uptake	Initial Concentration (mg L^{-1})	% Uptake
100	98.87 (25 min)	100	98.62 (30 min)	100	99.50 (30 min)
250	98.83 (5 min)	250	94.12 (30 min)	250	97.93 (30 min)
500	92.32 (5 min)	500	80.75 (30 min)	500	87.27 (30 min)
750	83.49 (30 min)	750	68.83 (20 min)	750	84.31 (30 min)
1000	83.05 (5 min)	1000	81.90 (30 min)	1000	81.99 (25 min)

bacteria. For example, an inhibition zone of 19 ± 0 mm was observed against the *K. pneumoniae* subsp. *pneumoniae* ATCC 13,883 strain. Additionally, inhibition zones of 13.5 ± 0.7 mm and 11.7 ± 0.6 mm were observed for MRSA and VRE strains, respectively. Inhibition zones of 18.7 ± 0.6 mm were observed for *P. vulgaris* RSKK 96029 highlighting the broad-spectrum effectiveness of bio waste against various bacterial strains.[44]

In the study conducted by Wu et al., the antibacterial effects of spherical-shaped copper nanoparticles against UTI pathogens, including *E. coli, Enterococcus* sp., *Proteus* sp., and *Klebsiella* sp., were evaluated. The inhibition zones around the copper nanoparticle-loaded discs were noted and measured. Their results indicate that copper nanoparticles exhibited significant activity against *E. coli* and *Enterococcus* sp., with large inhibition zones of 22.2 and 20.3 mm in diameter, respectively. *Klebsiella* sp. demonstrated moderate inhibition (18.5 mm), while *Proteus* sp. exhibited lower sensitivity to copper nanoparticles, with an inhibition zone of 16.33 mm[54] Additionally, the inhibition zones observed with CuNPs in *E. canadensis* were also substantial. However, the biowaste oil results showed similar outcomes to those observed with *P. vulgaris* (18.7 mm) (Table 4).

Samal et al. evaluated the antibacterial activity of silver nanoparticles (Pm-AgNPs) derived from *Pterocarpus marsupium* using the agar well diffusion technique against four multidrug-resistant bacterial isolates. The maximum zone of inhibition was observed against *S. aureus* with both the crude extract and Pm-Ag NPs, measuring 20 and 24 mm, respectively. MIC values for the crude extract and Pm-Ag NPs against *S. aureus* were 0.31 and 0.78 µg/mL, respectively, while MBC values were 1.24 and 3.12 µg/mL, respectively. The results from the agar well diffusion, MIC, and MBC assays for the other three bacterial strains indicate that Pm-Ag NPs exhibit higher inhibition activity compared to the crude bark extract.[55] Specifically, when compared to *E. canadensis*, the Pm-Ag NPs demonstrate a significantly higher antibacterial efficacy. Another notable study by Maldonado et al. investigated the antibacterial activities of two types of copper nanoparticles (CuNPs) derived from fresh leaves of *G. jasminoides*. The study compared CuNPs/RAFE and CuNPs/GJLE against *S. aureus* and *E. coli*. The results showed that CuNPs/RAFE did not support the growth of *S. aureus* at concentrations of 100 µg/mL or higher, demonstrating strong antibacterial activity. These concentrations were lower than those reported in previous studies. Conversely, CuNPs/GJLE allowed bacterial growth at all tested concentrations, with higher growth observed compared to the control. The observed resistance of *S. aureus* to CuNPs/GJLE was attributed to an increased expression of bacterial efflux pumps, which aid in the expulsion of Cu metal ions.[56]

A review of the extant literature reveals that the antibacterial potency of CuNPs synthesized using different plant extracts can vary. Although the antibacterial activity of plant extract-derived CuNPs is promising, it is essential to consider potential limitations and challenges. The observed variability in antibacterial efficacy depending on the type of plant extract used and the synthesis conditions indicates a necessity for standardization in production methods. Furthermore, additional research is necessary to comprehensively ascertain the long-term implications and safety of CuNPs in medical and environmental applications. Notwithstanding the challenges previously mentioned, the incorporation of CuNPs derived from plants into antimicrobial strategies provides a sustainable and effective approach to combating bacterial infections.

3.3. Adsorption Results

The removal efficiency in the adsorption experiments quantifies how effectively *E. canadensis* AC on MB from solution. Solutions with MB concentrations of 100, 250, 500, 750, and 1000 mg L^{-1} were mixed with the *E. canadensis* AC adsorbent, and contact times ranged from 5 to 30 min. These experiments were designed to evaluate the effect of contact time on the efficiency of MB removal. In adsorption research, temperature is an important variable. Experiments were carried out at 20 and 40 °C with a contact time of 30 min to assess its effect on MB adsorption. The agitation speed (200 rpm), adsorbent dosage (0.1 g), and pH (7.00) were maintained constants. Figure 7 displays the curve that was created by plotting the amount adsorbed against temperature. At 20 °C, removal efficiency ranged from 83.05% to 98.87%, with the highest efficiency of 98.87% for 100 mg L^{-1} MB after 25 min. At 30 °C, the efficiency varied from 68.83% to 98.62%, with the lowest efficiency of 68.83% observed for 750 mg L^{-1} MB after 20 min. At 40 °C, the efficiency ranged from 81.99% to 99.50%, peaking at 99.50% for 100 mg L^{-1} MB after 30 min. The data indicate that higher temperatures improve the removal efficiency, while higher initial concentrations can reduce efficiency, likely due to saturation effects or limited adsorption

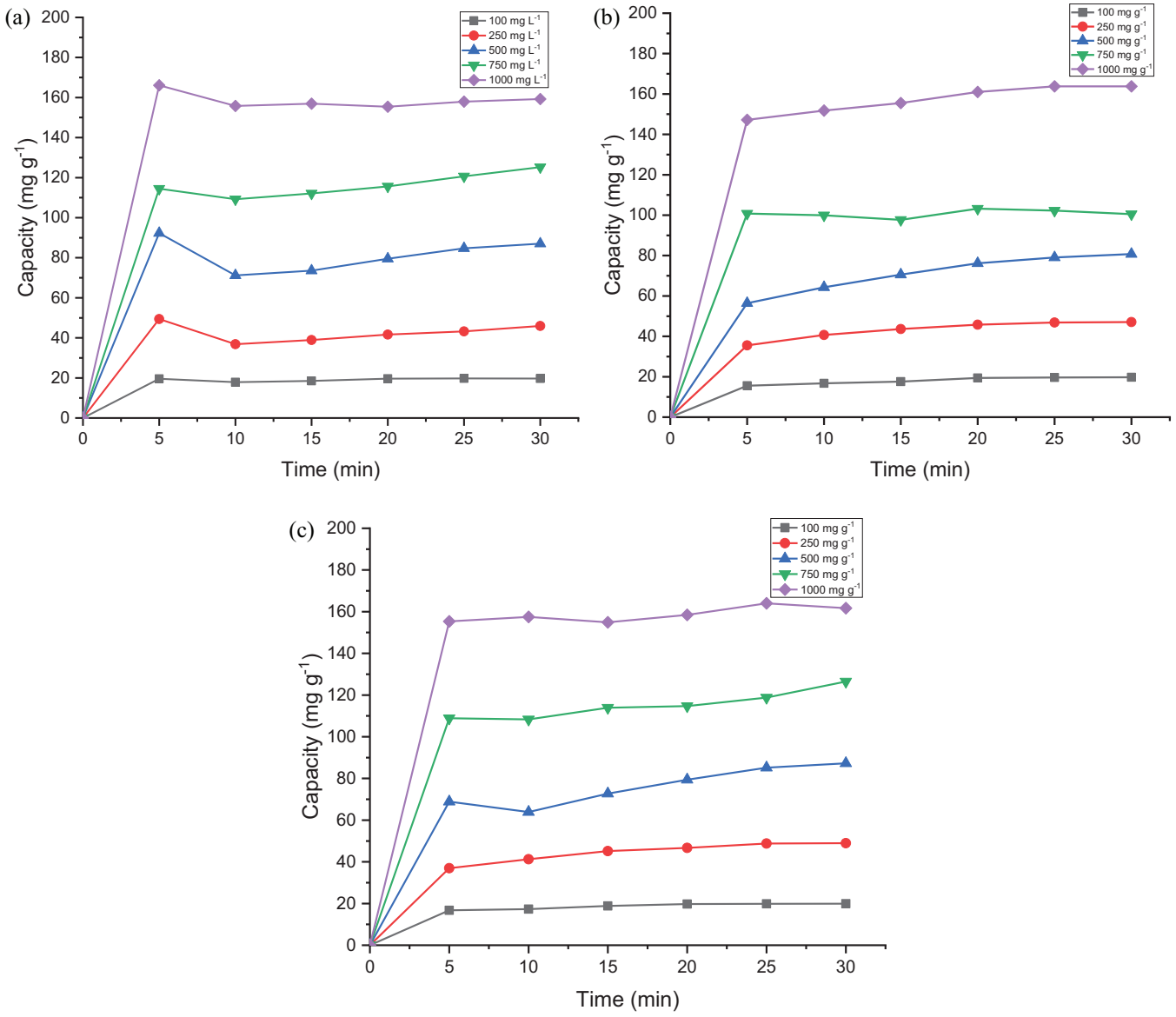

Figure 7. Graphs of adsorption capacity for the *E. canadensis* AC. a) 20 °C, b) 30 °C, and c) 40 °C.

sites. These results highlight the interplay between temperature, concentration, and removal efficiency, emphasizing the need to optimize these factors to enhance the performance of the AC in MB removal.

BET

The initial BET surface area of *E. canadensis* was determined to be 1105.277 m^2/g, indicating a specific surface area. This increase in surface area can be attributed to the larger total pore volume, estimated at 10.87 cc/g.[57]

Figure 8 illustrates the resulting N_2 adsorption–desorption isotherms and the pore size distribution curve. The isotherm for *E. canadensis* corresponds to a Type IV isotherm with an H4-type hysteresis loop, which is in accordance with the IUPAC classification. This specific hysteresis loop is typical of materials with an interconnected porous network, as explained by the Network Model.[58–60] In comparison, pure activated carbon also exhibited a Type IV isotherm and capillary condensation.

The desorption branches of the isotherms revealed pore size distribution curves (Figure 9) that indicate the carbon material possesses bimodal porosity. In particular, *E. canadensis* demonstrates pores with a prominent peak centered at approximately 9.62 nm, suggesting a well-dispersed and well-structured porous network.[61]

The isotherm and pore size distribution curves provide clear evidence that *E. canadensis* has undergone successful activation, resulting in a well-dispersed mesoporous structure. This result also matches with the XRD result.

4. Conclusion

This study highlights the significant potential of *E. canadensis* nanoparticles in terms of antioxidant properties. The low IC_{50} value obtained in the DPPH radical scavenging and iron chelat-

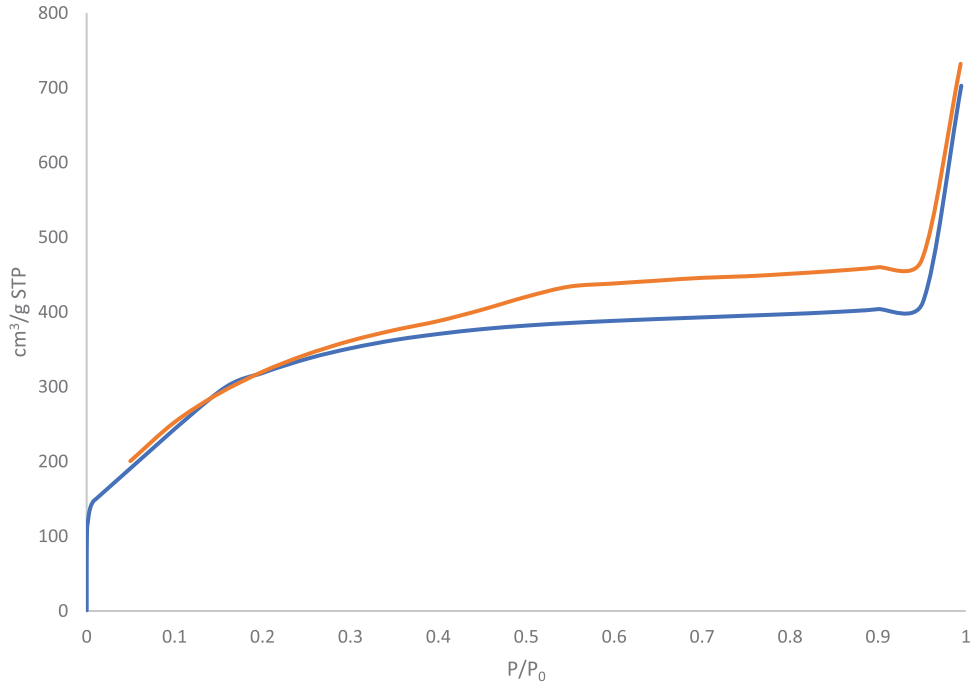

Figure 8. Isotherm data of *E. canadensis* AC.

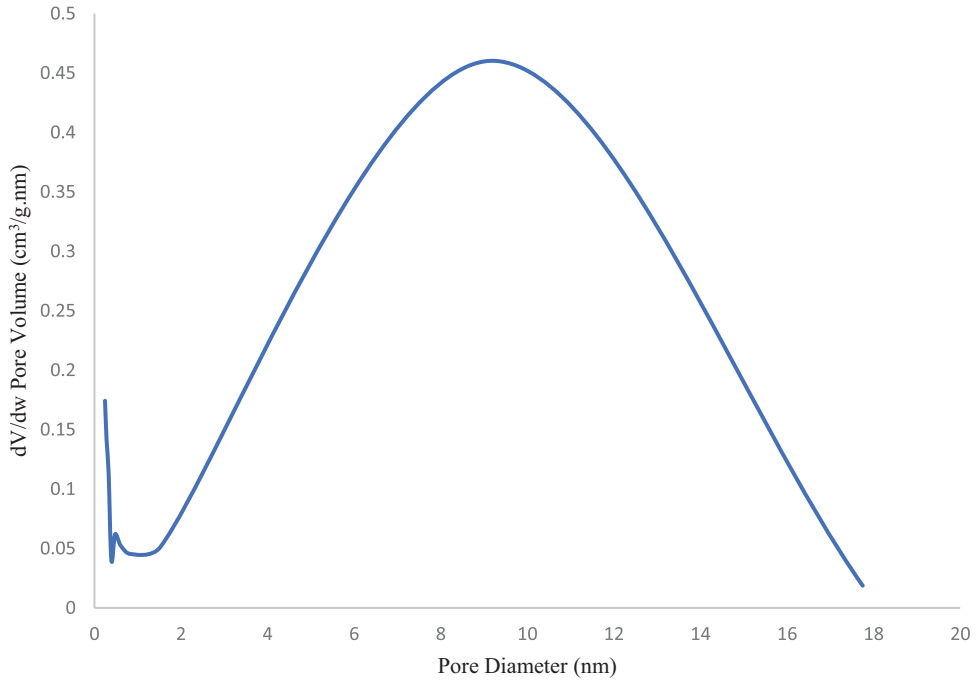

Figure 9. Pore size distribution curve of *E. canadensis* AC.

ing assay indicates the strong antioxidant capacity of these nanoparticles, positioning them as superior antioxidants compared to conventional CuNPs. This suggests that *E. canadensis* NPs could be valuable in treating conditions related to oxidative stress. However, the high free radical scavenging effect of activated carbon bio waste oil indicates that the antioxidant potential of this waste generated during activated carbon production can be used in various health-related issues.

Activated active carbon bio waste oil represents an innovative approach rooted in the zero-waste principle. This study found that activated carbon produced from oil waste displays significant antimicrobial efficacy against a broad spectrum of bacteria, including *P. vulgaris*, *K. pneumoniae*, and MRSA. By repurposing waste materials to produce this carbon, the approach not only supports environmental sustainability but also offers promising results as a potent antimicrobial agent. This

method contributes to waste management while minimizing the environmental impact associated with traditional production processes.

Future research should focus on exploring the detailed mechanisms underlying the antioxidant and antibacterial effects of *Erigeron canadensis* NPs and bio waste. Additionally, in vivo studies examining the biocompatibility and toxicity of these materials are essential for advancing their clinical applications. In line with the zero-waste principle, further modifications and developments of these materials should aim to enhance environmental and economic sustainability.

Overall, the promising results obtained from this study suggest that *Erigeron canadensis* NPs and bio waste provide a strong foundation for developing innovative and sustainable solutions within the healthcare sector, adhering to the zero-waste principle. The application potential of these materials extends from pharmaceutical formulations to food preservation and packaging systems, thereby contributing significantly to public health and environmental sustainability goals.

Author Contributions

Erdi Can Aytar: Formal analysis; Writing—original draft preparation. **Taşkın Basılı**: Formal analysis. **Alper Durmaz**: Formal analysis; Writing—original draft preparation. **Betül Aydın**: Formal analysis. **Rukan Can Seyfeli**: Formal analysis. **İbrahim Mizan Kahyaoğlu**: Formal analysis; Writing—original draft preparation. **Selcan Karakuş**: Writing—review and editing draft and supervision.

Acknowledgements

The authors have nothing to report.

Conflict of Interests

The authors declare no conflict of interest.

Data Availability Statement

The data that support the findings of this study are available from the corresponding author upon reasonable request.

Keywords: Antibacterial property · Antioxidant capacity · Cuo nanoparticles

[1] S. Saqib, A. Muneer, R. Munir, M. Sayed, M. Waqas, T. Aliyam, F. Younas, M. A. Farah, M. F. Elsadek, S. Noreen, *Environ. Res.* **2024**, *259*, 119569.
[2] H. Ganji, M. Taghavijeloudar, *Environ. Res.* **2024**, *259*, p. 119529.
[3] S. Escudero-Curiel, U. Penelas, M. Á. Sanromán, M. Pazos, *Chemosphere* **2021**, *268*, 129318.
[4] M. D. A. Islam, M. K. Nazal, A. A. Akinpelu, M. Sajid, N. A. Alhussain, R. E. I. K. Billah, L. Bahsis, *Diam. Relat. Mater.* **2024**, *147*, 111375.
[5] S. K. Heena, A. Kalia, H. Panwar, V. Kaur, *Biocatal. Agric. Biotechnol.* **2024**, *57*, 103104.
[6] M. Srivastava, K. R. B. Singh, T. Singh, M. Asiri, M. Suliman, H. Sabia, P. R. Deen, R. Chaube, J. Singh, *Int. J. Biol. Macromol.* **2023**, *253*, 126886.
[7] N. Verma, D. Pathak, N. Thakur, *Next Materials* Oct. **2024**, *5*, 100271.
[8] H. Adugna, D. Ezez, A. Guadie, M. Tefera, *J. Agric. Food Res.* **2024**, *16*, 101190,.
[9] Y. Fu, J. Li, M. Almasi, *ChemistrySelect* **2023**, *8*, e202204841, https://doi.org/10.1002/SLCT.202204841.
[10] Y. Teng, Y. Li, D. Yu, Y. A. N. Meng, Y. Wu, X. Zhao, X. Liu, *ChemistrySelect* **2019**, *4*, 956–962.
[11] K. Mohammadi, M. A. Sani, M. Azizi-Lalabadi, D. J. McClements, *Adv. Colloid Interface Sci.* **2022**, *307*, 102734.
[12] Gunture, T. Y. Lee, *J. Environ. Chem. Eng.* **2024**, *12*, 113759.
[13] B. W. Ike, J. Alake, E. O. Akintemi, D. K. Adu, Z. Nate, R. Chauhan, L. Miya, R. Karpoormath, M. Faya, *J. Mol. Struct.* **2024**, *1315*, 138988.
[14] L. Zhang, Q. Xu, L.i Li, L.u Lin, J. Yu, J. Zhu, H. Zhang, G. Xia, H. Zang, *Ind. Crops Prod.* **2020**, *148*, 112283.
[15] I. Pawlaczyk, L. Czerchawski, W. Kuliczkowski, B. Karolko, W. Pilecki, W. Witkiewicz, R. Gancarz, *Thromb. Res.* **2011**, *127*, 328–340.
[16] A. Hussain, A. Zahid, S. Ali, N. Khalid, A. Ashraf, A. Latif, M. A. Farrukh, M. Jabeen, *J. Taiwan Inst. Chem. Eng.* **2024**, *163*, 105642.
[17] C. Kandasamy, B. Balasubramanian, P. Prakash, R. Baskaran, H. Kamyab, S. Chelliapan, N. Arjunan, *J. Taiwan Inst. Chem. Eng.* **2024**, *166*, 105602.
[18] S. Rani, P. Kumar, N. Kataria, *J. Taiwan Inst. Chem. Eng.* **2024**, 105566, https://doi.org/10.1016/J.JTICE.2024.105566.
[19] Pratibha, K. R., A. Singhal, R. Meena, A. Kumari, *J. Herb. Med.* **2024**, *44*, 100859.
[20] C. Thummaneni, R. Lavu, R. Golli, D. Divya Pabbathi, G. Jayasri, M. Vangalapati, *Mater. Today Proc.* **2023**, *80*, 1645–1649.
[21] G. K. Reen, P. Sharma, A. Kumar, *Nanotechnology Based Strategies for Combating Antimicrobial Resistance* (Eds: M. Y. Wani, I. A. Wani, A. Rai), Springer, Singapore **2024**.
[22] P. Kaushal, D. Maity, R. Awasthi, *J. Drug Deliv. Sci. Technol.* **2024**, *94*, 105488.
[23] S. Kumaravel, M. Geetha, T. Niyitanga, D. S. Kumar, M. M. Al-Ansari, R. Mythili, S. Suganthi, L. Guganathan, A. Murugan, S. Ragupathy, *Process Saf. Environ. Prot.* **2024**, *188*, 1338–1345.
[24] L. A. Cavazos-Cuello, R. Ocampo-Pérez, S. Tututi-Ávila, N. E. Dávila-Guzmán, E. Soto-Regalado, J. J. Salazar-Rábago, *Chem. Eng. Res. Des.* **2023**, *199*, 152–161.
[25] A. Melliti, M. Yılmaz, M. Sillanpää, B. Hamrouni, R. Vurm, *Colloids Surf. A Physicochem. Eng. Asp.* **2023**, *672*, 131775.
[26] S. Suresh, V. C. Srivastava, I. M. Mishra, A. Pratap-Singh, *J. Environ. Chem. Eng.* **2021**, *9*, 104843.
[27] L. Domergue, N. Cimetière, S. Giraudet, P. L.e Cloirec, *J. Environ. Chem. Eng.* **2022**, *10*, 108218.
[28] E. C. Aytar, *Chem. Biodivers.* **2024**, *21*, e202401057.
[29] A. Braca, N. de Tommasi, L. di Bari, C. Pizza, M. Politi, I. Morelli, *J. Nat. Prod.* **2001**, *64*, 892–895.
[30] T. C. P. Dinis, V. M. C. Madeira, L. M. Almeida, *Arch. Biochem. Biophys.* **1994**, *315*, 161–169.
[31] N. J. Tamanna, M. Sahadat Hossain, N. M. Bahadur, S. Ahmed, *Results Chem* **2024**, *7*, 101313.
[32] M. Sahadat Hossain, S. Ahmed, *Results in Materials* **2023**, *20*, 100492.
[33] E. Tan, İ. M. Kahyaoğlu, Selcan Karakuş, *Polym. Bull.* **2022**, *79*, 7363–7389.
[34] R. Aziz, M. Saad, H. Tahir, R. Aziz, *Surfaces and Interfaces* **2024**, *44*, 103725.
[35] S. Suresh, S. Karthikeyan, K. Jayamoorthy, *Journal of Science: Advanced Materials and Devices* **2016**, *1*, 343–350,.
[36] S. Chandra, *Journal of Medicinal Plants Studies* **2019**, *7*, 82–85.
[37] A. Fellah, P. Anjukandi, M. R. Waterland, M. A. K. Williams, *Carbohydr. Polym.* **2009**, *78*, 847–853.
[38] E. N. Dubis, A. T. Dubis, J. W. Morzycki, *J. Mol. Struct.* **1999**, *511–512*, 173–179, https://doi.org/10.1016/S0022-2860(99)00157-X.
[39] P. S. Sundaram, T. Sangeetha, S. Rajakarthihan, R. Vijayalaksmi, A. Elangovan, G. Arivazhagan, *Physica B Condens. Matter* **2020**, *595*, 412342.
[40] R. Venugopalan, S. Pitchai, K. Devarayan, V. C. Swaminathan, *Mater. Today Proc.* **2020** *33*, 4023–4025.
[41] S. M. Hasheminya, J. Dehghannya, *Part. Sci. Technol.* **2020**, *38*, 1019–1026.
[42] S. Golinejad, M. H. Mirjalili, H. Rezadoost, M. Ghorbanpour, *Ind. Crops Prod.* Feb. **2023**, *192*, 115988.

[43] J. Shanmugapriya, C. A. Reshma, V. Srinidhi, K. Harithpriya, K. M. Ramkumar, D. Umpathy, K. Gunasekaran, R. Subashini, *J. Nanomater.* Jan. **2022**, *2022*, no. p. 7967294.
[44] S. Rajeshkumar, S. Menon, S. Venkat Kumar, M. M. Tambuwala, H. A. Bakshi, M. Mehta, S. Satija, G. Gupta, D. K. Chellappan, L. Thangavelu, K. Dua, *J. Photochem. Photobiol. B* **2019**, *197*, 111531.
[45] M. A. Asghar, M. A. Asghar, *Int. J. Biol. Macromol.* **2020**, *160*, 1168–1176.
[46] M.-J. Lai, Y.-W. Huang, H.-C. Chen, L.i-l. Tsao, C.-F. Chang Chien, B. Singh, B. R. Liu, *Nanomaterials* **2022**, *12*, 3715.
[47] J. Ramos-Zúñiga, N. Bruna, J. M. Pérez-Donoso, *Int. J. Mol. Sci.* **2023**, *24*, 10503.
[48] E. Mavil-Guerrero, R. Vazquez-Duhalt, K. Juarez-Moreno, *Chemosphere* **2024**, *347*, 140713.
[49] R. K. Mishra, B. Gariya, P. Savvasere, D. Dhir, P. Kumar, K. Mohanty, *ACS Omega* **2024**, *9*, 25779–25792.
[50] T. Chorazy, J. Čáslavský, V. Žvaková, J. Raček, P. Hlavínek, *Waste Biomass Valorization* **2020**, *11*, 4491–4505.
[51] K. S. Singh, S. Nayak, E. Lalnunmawii, M. B. Devi, B. S. Shagolsem, S. Gouda, *J. Anal. Appl. Pyrolysis* **2024**, *180*, 106528.
[52] J. K. Patra, G. Das, J. W. Choi, K. H. Baek, *Foodborne Pathogens and Disease* **2016** *13*, 13–20.
[53] K. Riekkinen, V. Giannini, G. Moro, M. G. Marche, R. Hamze, L. Ruiu, *Forests* **2022**, *13*, 559.
[54] S. Wu, S. Rajeshkumar, M. Madasamy, V. Mahendran, *Artif Cells Nanomed. Biotechnol.* **2020**, *48*, 1153–1158.
[55] S. Samal, P. K. Das, D. Dubey, T. K. Rajwar, S. K. Swain, *Ind. Crops Prod.* **2024**, *209*, 117923.
[56] A. Nieto-Maldonado, S. Bustos-Guadarrama, H. Espinoza-Gomez, L. Z. Flores-López, K. Ramirez-Acosta, G. Alonso-Nuñez, R. D. Cadena-Nava, *J. Environ. Chem. Eng.* **2022**, *10*, 107130.
[57] V. Varadharajan, D. S. Senthilkumar, K. Senthilkumar, V. P. Sundramurthy, R. Manikandan, H. Senthilarasan, H. Ganesan, I. Kesavamoorthy, A. Ramasamy, *Journal of Water Process Engineering* **2022**, *49*, 103046.
[58] K. S. W. Sing, *Pure Appl. Chem.* **1985**, *57*, 603–619.
[59] M. Thommes, R. Köhn, M. Fröba, *Stud. Surf. Sci. Catal.*, **2002** *142*, 1695–1702.
[60] R. Can Seyfeli, D. Varisli, *Int. J. Hydrogen Energy* **2020**, *45*, 34867–34878.
[61] R. C. Seyfeli, D. Varisli, *Int. J. Hydrogen Energy* **2022**, *47*, 15175–15188.

Manuscript received: October 24, 2024